Neuron, Volume *72*

Supplemental Information

An Imbalancing Act: Gap Junctions Reduce the Backward Motor Circuit Activity to Bias *C. elegans* for Forward Locomotion

Taizo Kawano, Michelle D. Po, Shangbang Gao, George Leung,William S. Ryu, and Mei Zhen

Figure S1. **Calcium imaging in *C. elegans* premotor interneurons and motoneurons**

A, A schematic diagram of the imaging system for simultaneous calcium imaging and motion, and a flow chart of image processing and data analysis. Image capture, stage control and data storage are processed in real-time to track moving objects during recordings with in-house developed software. Raw data are processed post image capture by other customized algorithms to obtain profiles for neuronal activity and movement; B, An imaging profile of AVA in wild-type animals expressing a genetic calcium sensor cameleon. YFP and CFP signals show reciprocal changes when YFP/CFP ratio increases rapidly in the AVA premotor interneurons, indicating that these ratio changes reflect true FRET responses; C, Simultaneous calcium imaging of RIM and AVA showed similar calcium transient profiles, which supports their co-activation; D, Left panel, calcium transients of VB9 (red trace) and VA8 (blue trace) in a moving wild-type animal as shown in Figure 2A. This animal frequently switched directions during the recording. The large YFP/CFP ratio changes exhibited by VA8 (the blue trace in the left panel), often coinciding with switching directions, reflected FRET signals, as shown by reciprocal changes between YFP and CFP signals. a.u. arbitrary unit.

Figure S2. A, Restoring the B>A pattern rescued continuous forward motion in innexin mutants. The averaged duration time for forward and backward movements (upper graphs), and the total percentage of time, or the propensity of animals in forward and backward motion or pause (lower graphs) for each genotype. *unc-7* animals expressing the A motoneuron silencing transgene (P*unc-4::TWK-18(gf))* exhibited an increased duration of continuous forward movement and decreased duration for backing (upper graphs), as well as an increased propensity for forward motion and a reduced propensity for backing (lower graphs). **B. Reducing B motoneuron output in wild-type animals reduced forward motion and increased backing.** Wild-type animals with a reduced B motoneuron output, by reducing either B activity (P*acr-5::TWK-18(gf)*), or AVB activity (P*sra-11::TWK-18(gf)*), exhibited a decreased duration of continuous forward movement (upper graphs), a decreased propensity for forward movement, concomitant with an increased propensity for backing (lower graphs). Propensity analyses were carried out using pooled data from animals (N>10) per genotype. *** P<0.001, ** P<0.01, * P<0.05 by the Mann-Whitney U test. Error bars: SEM.

Figure S3

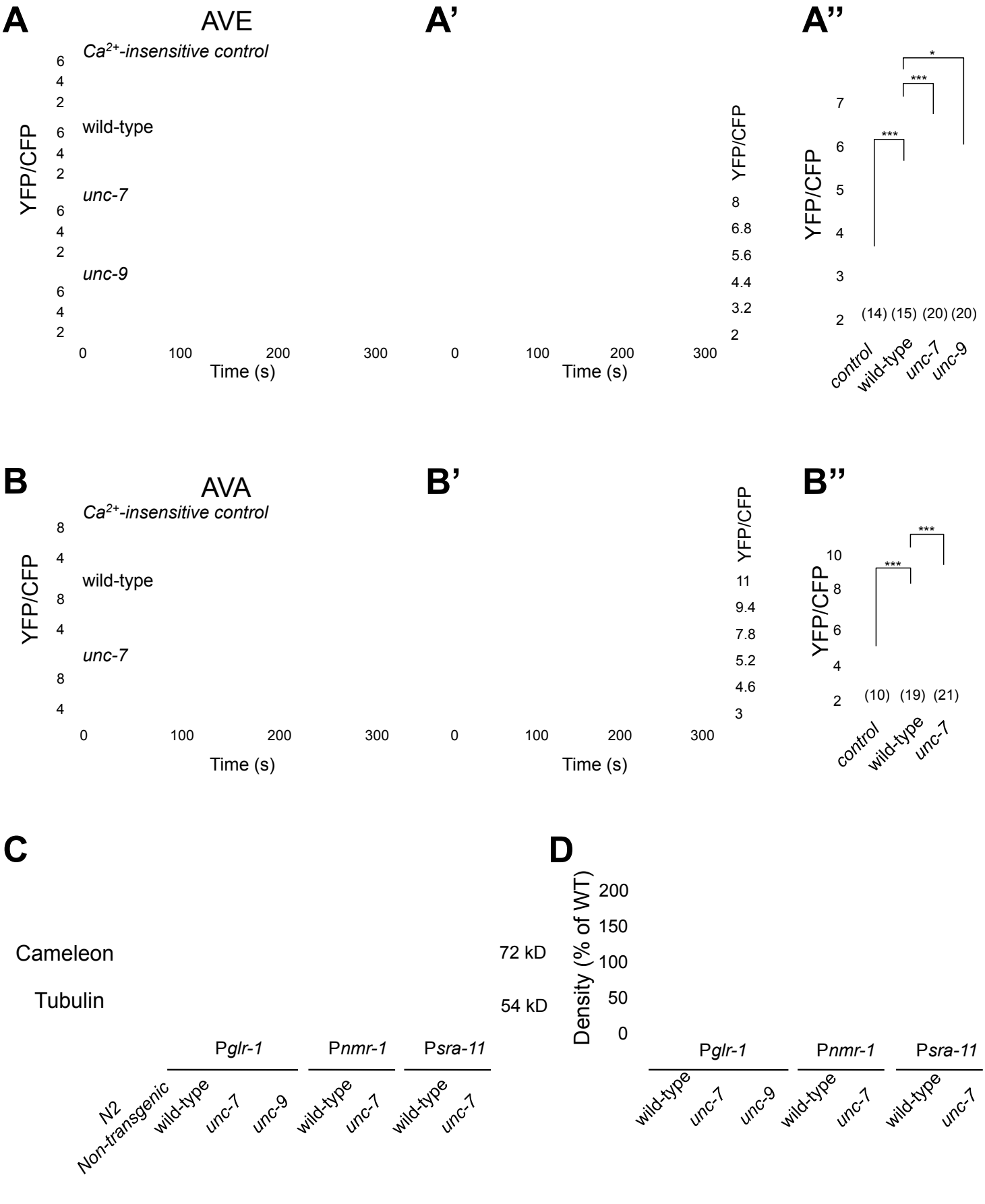
A
AVE
A'
A''
Ca2+-insensitive control
wild-type
unc-7
unc-9
YFP/CFP
Time (s)
(14) (15) (20) (20)
control
wild-type
unc-7
unc-9
B
AVA
B'
B''
(10) (19) (21)
C
Cameleon
Tubulin
72 kD
54 kD
Pglr-1
Pnmr-1
Psra-11
N2
Non-transgenic
D
Density (% of WT)

Figure S3. Imaging of AVE and AVA separately under a restricted movement condition also showed an increased activity of these interneurons in *unc-7* mutants

A-B, Representative calcium transient traces in AVE (A) and AVA (B) of each genotype recorded under identical experimental conditions; A'-B', Raster plots of calcium traces, each horizontal line corresponding to the YFP/CFP ratio of an animal of the respective genotypes as in the left panels during five minute recording, pseudo-colored according to the calcium transient level over time in AVE (A') and AVA (B'); A''- B'', Mean and distribution of the calcium transient level of each genotype in AVE (A'') and AVA (B''). Each data point represents the averaged YFP/CFP ratio during the five-minute recording for each animal. N for each genotype is shown in brackets. *** $p < 0.001$, ** $p < 0.01$, * $p < 0.05$ by the Mann-Whitney U test; C-D, Expression levels of calcium sensors did not changed in *unc-7* and *unc-9* mutant background. (C) a representative result for western blot analyses of synchronized strains expressing interneuron cameleon calcium sensors used in this study; (D) the density ratio cameleon/Tubulin in each genotype, normalized against that of the ratio in wild-type animals, for each reporter. N=2. Error bars represent SEM.

Figure S4

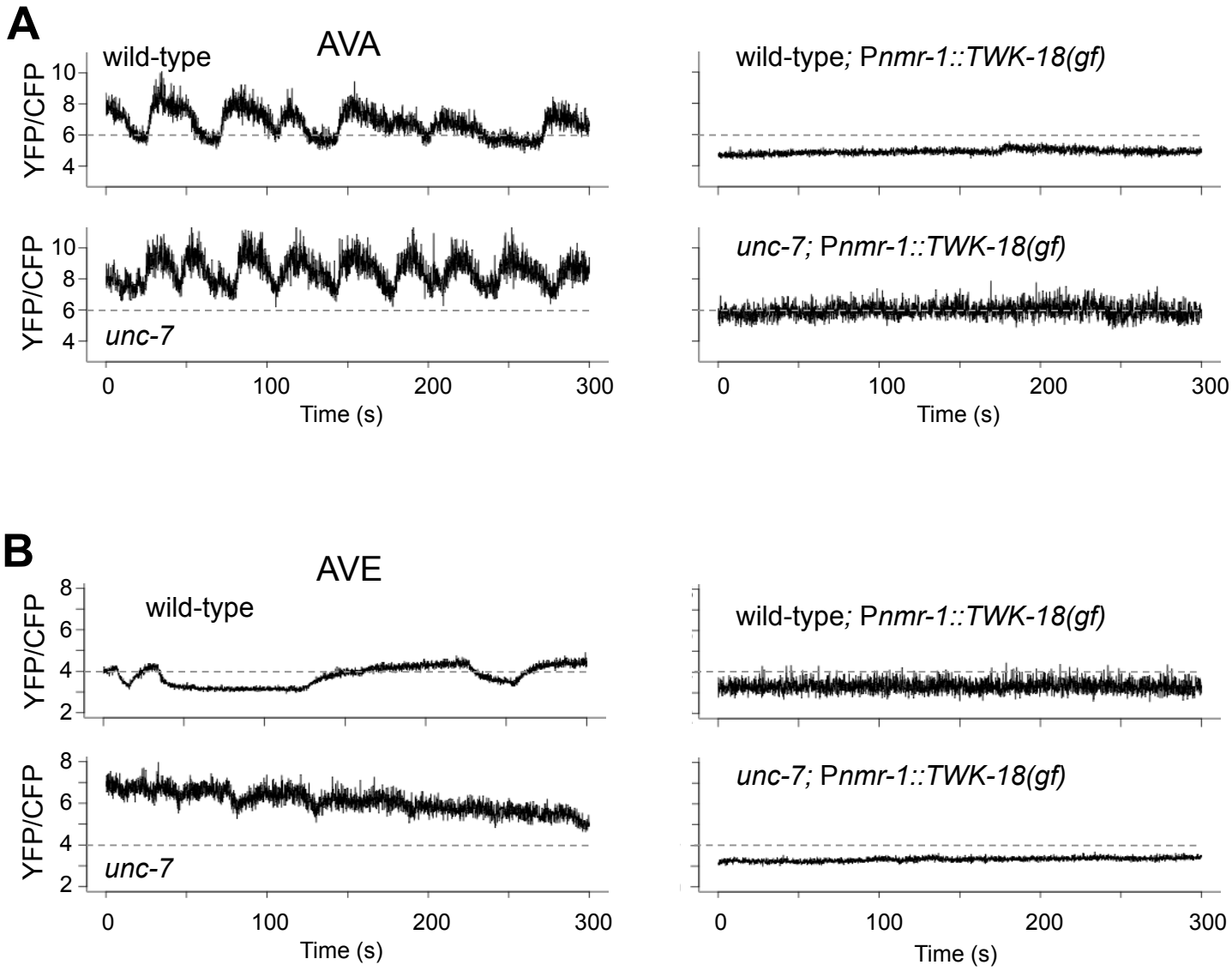
A
AVA
wild-type
YFP/CFP
10
8
6
4
unc-7
wild-type; Pnmr-1::TWK-18(gf)
unc-7; Pnmr-1::TWK-18(gf)
0
100
200
300
Time (s)
B
AVE
wild-type
YFP/CFP
8
6
4
2
unc-7
wild-type; Pnmr-1::TWK-18(gf)
unc-7; Pnmr-1::TWK-18(gf)
0
100
200
300
Time (s)

Figure S4. The P*nmr-1::TWK-18(gf)* transgene effectively silences the activity of backward premotor interneurons in wild-type animals and *unc-7* mutants.

Representative calcium transient traces of premotor interneurons, AVA (A) and AVE (B), in animals without (left panels), or with (right panels) the P*nmr-1::TWK-18(gf)* transgene. *TWK-18*(*gf)* expression in imaged neurons was monitored and confirmed by the RFP signal co-expressed from the bi-cistronic transcript.

Figure S5

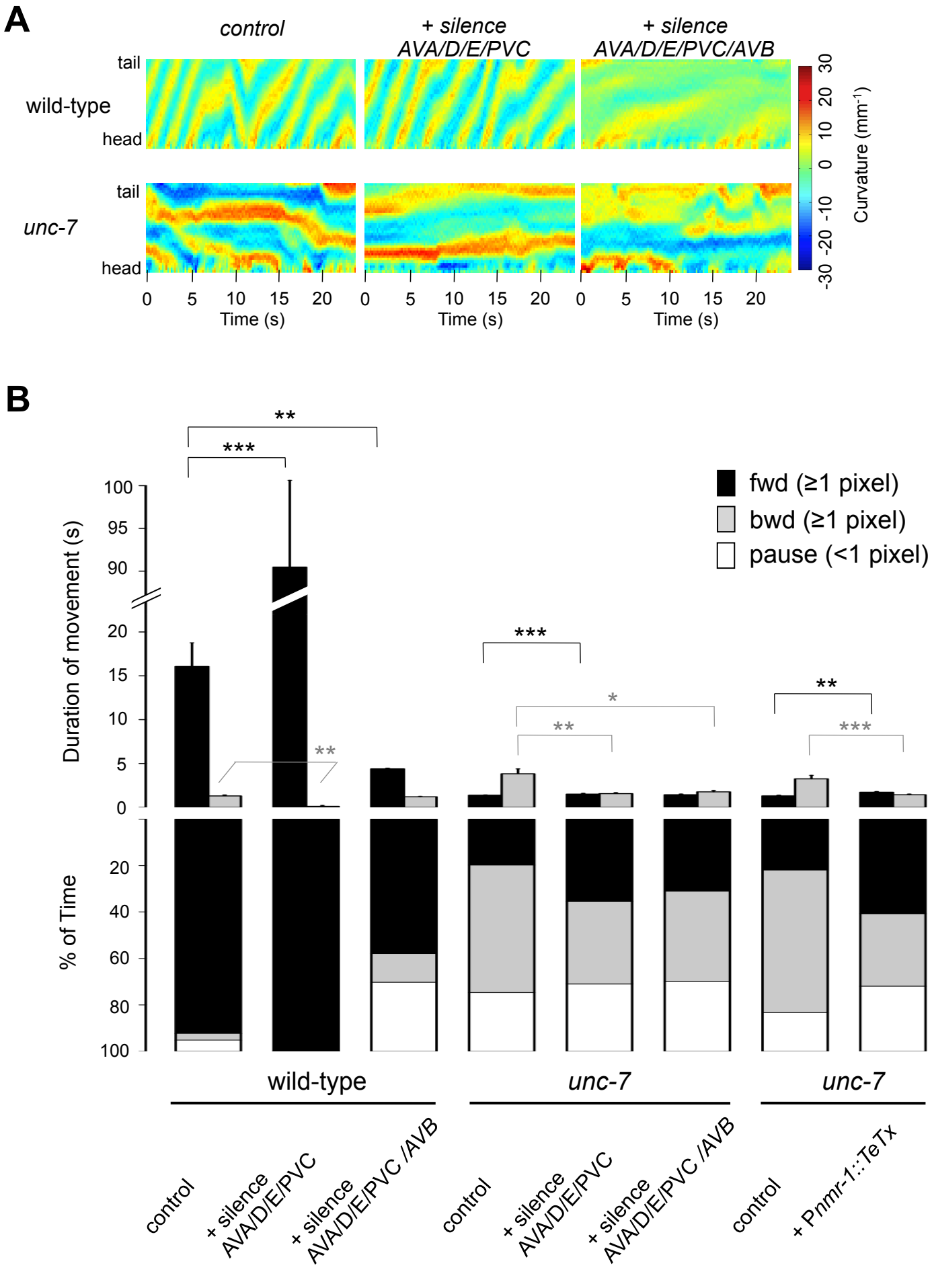
A
control
+ silence AVA/D/E/PVC
+ silence AVA/D/E/PVC/AVB
wild-type
unc-7
tail
head
0 5 10 15 20
Time (s)
Curvature (mm-1)
-30 -20 -10 0 10 20 30
B
fwd (≥1 pixel)
bwd (≥1 pixel)
pause (<1 pixel)
Duration of movement (s)
% of Time
wild-type
unc-7
unc-7
control
+ silence AVA/D/E/PVC
+ silence AVA/D/E/PVC /AVB
control
+ silence AVA/D/E/PVC
+ silence AVA/D/E/PVC /AVB
control
+ Pnmr-1::TeTx

Figure S5. Manipulating premotor interneuron activity does not rescue *kinking* in innexin mutants. A, the representative body posture during movement, shown by curvature analyses, of wild-type (upper panels) and *unc-7* (lower panels) animals that expressed different neuronal silencer transgenes. *TWK-18(gf)* was expressed either by P*nmr-1* to reduce the activity of the backward circuit premotor interneurons and PVC (+ silence AVA/D/E/PVC), or by both P*nmr-1* and P*sra-11* to reduce the activity of all premotor interneurons (+ silence AVA/D/E/PVC/AVB). *kinking*, represented by distorted, discontinuous, deep body bends, could not be rescued by either transgene in these innexin mutants. B, a quantification of directional movement for animals of the respective genotypes in A. Upper graphs represent the averaged duration time of forward and backward movements; the matching lower graphs represent the total percentage of time that these animals spent in forward or backward motion (movement ≥1 pixel) or pausing (movement <1 pixel). In wild-type animals, reducing the activity of backward premotor interneurons and PVC (silencing AVA/D/E/PVC) led to a switch to an almost exclusive forward movement (black bars). Innexin mutants expressing the same transgene however failed to execute continuous forward movements (black bar, upper graph), despite reducing their propensity and duration for backing (grey bars, upper and lower graph). In *unc-7* mutants, reducing the activity of all premotor interneurons decreased the propensity and duration for backing (grey bars, upper and lower graph), but it did improve the duration of forward movement (black bar, upper graph). Blocking chemical synaptic output from backward premotor interneurons (AVA, AVE, AVD) and PVC (+*Pnmr-1*::TeTx) also reduced propensity and duration of backing in *unc-7* mutants. *** P<0.001 by the Mann-Whitney U test. Error bars: SEM.

Figure S6

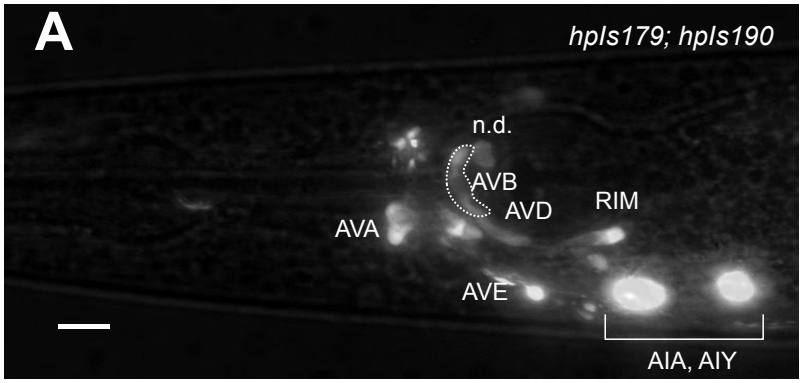
A
hpIs179; hpIs190
n.d.
AVB
AVD
RIM
AVA
AVE
AIA, AIY

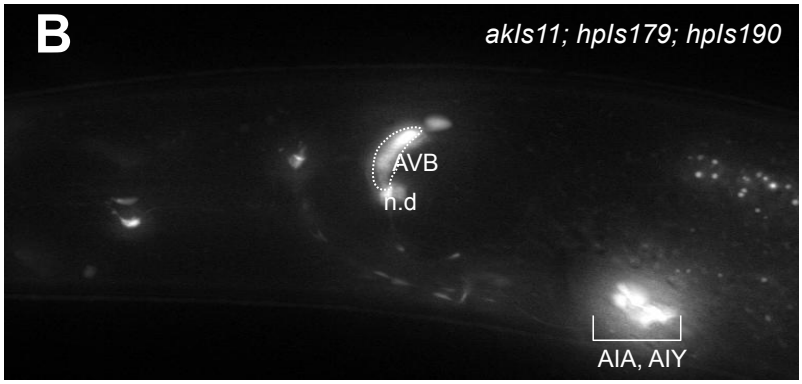
B
akIs11; hpIs179; hpIs190
AVB
n.d
AIA, AIY

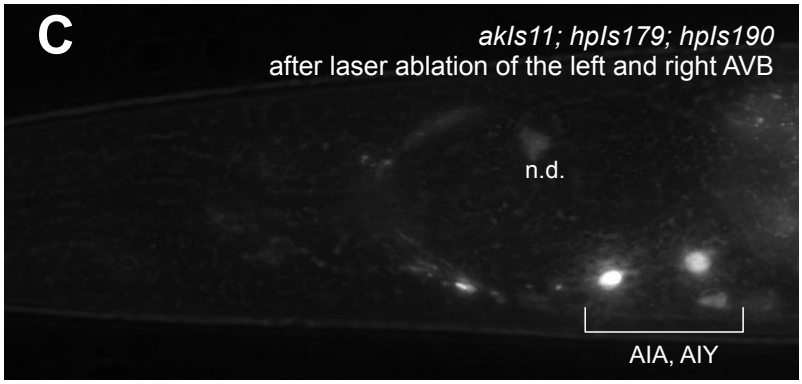
C
akIs11; hpIs179; hpIs190
after laser ablation of the left and right AVB
n.d.
AIA, AIY

Figure S6. The anatomic removal of five pairs of premotor interneurons in wild-type animals. A, premotor interneurons in the head region (arrowheads) were labeled with fluorescent signals in a double transgenic animal *hpIs190 (*P*nmr-1::D3cpv); hpIs179 (*P*sra-11::D3cpv)*; B, in a triple transgenic animal *akIs11 (*P*nmr-1::ICE); hpIs190; hpIs179*, backward premotor interneurons and PVC (located in the tail region, not shown) were absent, but AVBs were intact; C, a young adult animal with the AVB neuron pair laser ablated in the *akIs11; hpIs190; hpIs179* background during the second larval stage. n.d. an unidentified pharyngeal neuron, possibly I4. Scale bar: 5μm.

Figure S7

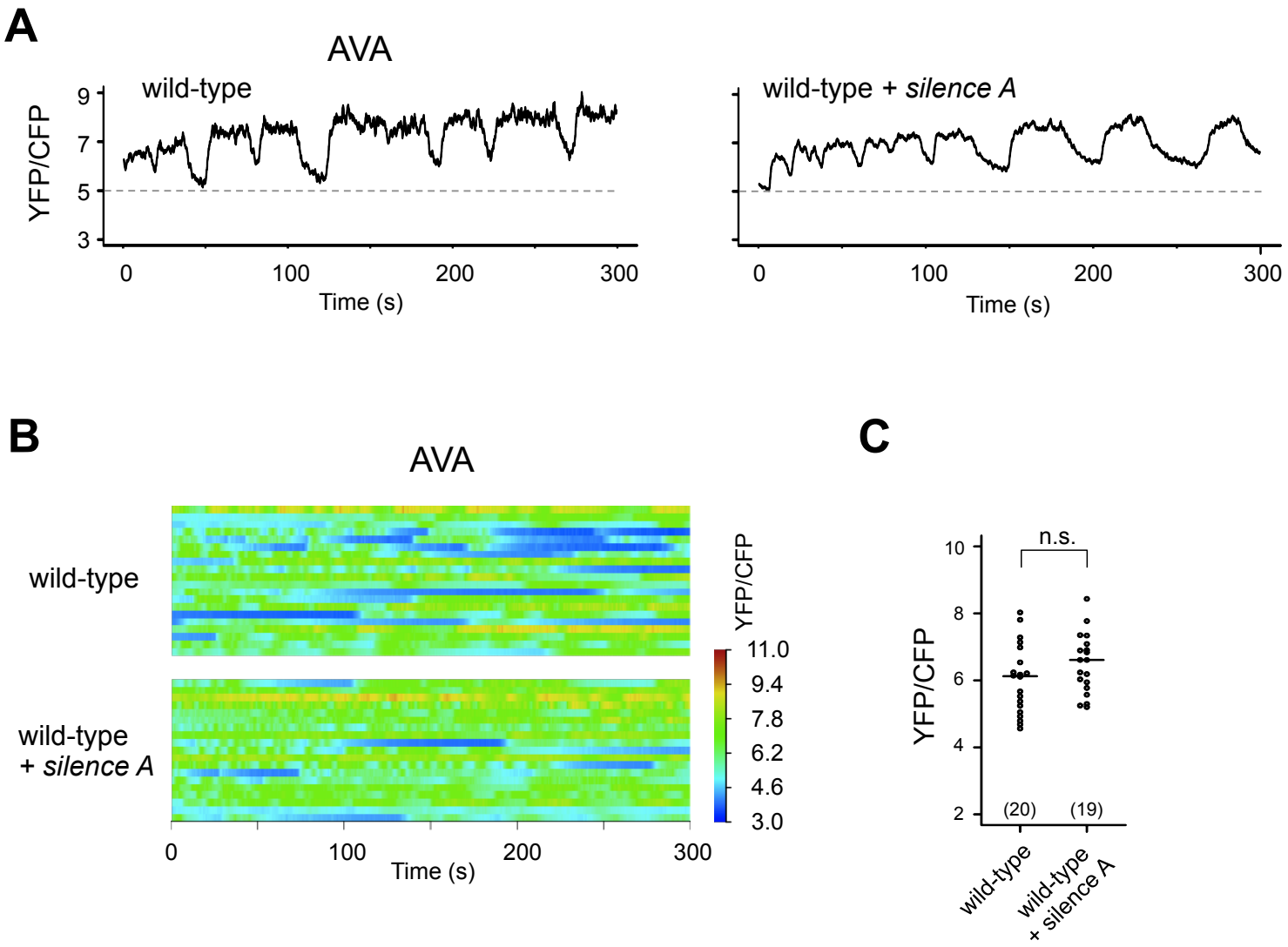
A
AVA
wild-type
wild-type + *silence A*
YFP/CFP
9
7
5
3
0
100
200
300
Time (s)
B
AVA
wild-type
wild-type
+ *silence A*
0
100
200
300
Time (s)
YFP/CFP
11.0
9.4
7.8
6.2
4.6
3.0
C
n.s.
YFP/CFP
10
8
6
4
2
(20)
(19)
wild-type
wild-type
+ silence A

Figure S7. Silencing the A-class motoneurons by *TWK-18*(*gf*) failed to reduce the activity of AVA premotor interneurons in wild-type animals A, Representative traces of the AVA calcium transients in wild-type animals without (left panel) or with (right panel) the same P*unc-4::TWK-18(gf)* transgene that effectively reduced A-motoneuron activity (Figure 4D) and prevented backward movement; B, Raster plot of the calcium transients for wild-type animals without and with the P*unc-4::TWK-18(gf)* transgene; C, a mean and distribution of the calcium transient level of wild-type animals without and with the P*unc-4::TWK-18(gf)* transgene. There was no decrease of the AVA calcium transient level in the presence of the hyperpolarizing transgene P*unc-4::TWK-18(gf)*.

Experimental Procedures:

A list of constructs and transgenes generated for this study

Plasmid	Description	Transgenes Used For Data in Figures
pJH1579	P*glr-1::YC3.60*	*hpEx1599* and *hpIs157*
pJH1737	P*glr-1::Ca^{2+}-insensitive YC3.60*	*hpEx1740*
pJH1969	P*nmr-1::D3cpv*	*hpEx1912* and *hpIs190*
pJH1973	P*sra-11::D3cpv*	*hpEx1926* and *hpIs179*
pJH1863	P*acr-2::D3cpv*	*hpEx1911* and *hpIs171*
pJH2157	P*acr-2::Ca^{2+}-insensitive D3cpv*	*hpEx2314*
pJH1556	P*glr-1::UNC-7::Cerulean*	*hpEx1577*
pJH1924	P*nmr-1::UNC-7-UrSL-wCherry*	*hpEx1968*
pJH2085	P*nmr-1::UNC-7::GFP*	*hpEx2090*
pJH2452	P*rig-3::UNC-7-UrSL-wCherry*	*hpEx2457*
pJH2037	P*sra-11::UNC-7-UrSL-wCherry*	*hpEx2312*
pJH2133	P*opt-3::UNC-7-UrSL-wCherry*	*hpEx2110*
pJH1898	P*acr-2::UNC-7-UrSL-wCherry*	*hpEx1888*
pJH1982	P*sto-6::UNC-7-UrSL-wCherry*	*hpEx2066*
pJH2165	P*unc-4::UNC-7-UrSL-wCherry*	*hpEx2081*
pJH2164	P*acr-5::UNC-7-UrSL-wCherry*	*hpEx2082*
pJH1848	P*glr-1::UNC-9-UrSL-wCherry*	*hpEx1825*
pJH2069	P*nmr-1::UNC-9-UrSL-wCherry*	*hpEx2114*
pJH1897	P*acr-2::UNC-9-UrSL-wCherry*	*hpEx2094*
pJH1981	P*sto-6::UNC-9-UrSL-wCherry*	*hpEx2065*
pJH2141	P*unc-4::UNC-9-UrSL-wCherry*	*hpEx2087*
pJH2140	P*acr-5::UNC-9-UrSL-wCherry*	*hpEx2086*
pJH2106	P*nmr-1::TWK-18(gf)-UrSL-wCherry*	*hpEx2330*
pJH2217	P*sra-11::TWK-18(gf)-UrSL-wCherry*	*hpEx2026*
pJH2108	P*unc-4::TWK-18(gf)-UrSL-wCherry*	*hpEx2171*

pJH2106 /pJH2217	P*nmr-1::TWK-18(gf)-UrSL-wCherry* + P*sra-11::TWK-18(gf)-UrSL-wCherry*	*hpEx2329*
pJH2085 /pJH2141	P*nmr-1::UNC-7::GFP* + P*unc-4::UNC-9-UrSL-wCherry*	*hpEx2090*
pJH2069 /pJH2165	P*nmr-1::UNC-9-UrSL-wCherry* + P*unc-4::UNC-7-UrSL-wCherry*	*hpEx2028*
pJH2217	P*sra-11::TWK-18-UrSL-wCherry*	*hpEx2454*
pJH2107	P*acr-5::TWK-18-UrSL-wCherry*	*hpEx2255*
pJH1824	P*rig-3::wCherry*	*hpEx2414*
pJH2644	P*nmr-1::TetanusToxin-UrSL-wCherry*	*hpEx2616*

Molecular Biology

All promoters used in this study were generated by PCR-amplification using *C. elegans* N2 genomic DNA as a template. Promoters included a 5.3 kb P*glr*-1 (Maricq et al., 1995) , 5.1 kb P*nmr-1* (Brockie et al., 2001) , 2.5 kb P*opt-3* (Fei et al., 2000) , 4.8 kb P*rig-3* (Wormbase), 2.8 kb P*sra-11* (Troemel et al., 1995), 3.4 kb P*acr-2* (Jospin et al., 2009), 2.2 kb P*sto-6* (Po and Zhen, unpublished), 2.5 kb P*unc-4* (Miller et al., 1992) and 4.3 kb P*acr-5* (Winnier et al., 1999) genomic DNA sequence upstream of the ATG start codon of each gene, respectively. The P*nmr-1* promoter used in this study excludes a 2 kb fragment encoding *cex-1* that interferes with calcium imaging (Kawano and Zhen, unpublished observation). Intercistronic region consisting of a U-rich element and Splice Leader sequence (UrSL) between *gpd-2* and *gpd-3* was PCR amplified with OZM2301 (AAG CTA GCG AAT TCG CTG TCT CAT CCT ACT TTC ACC) and OZM2302 (AAG GTA CCG ATG CGT TGA AGC AGT TTC CC) using pBALU14 (Tursun et al., 2009) as a template, and inserted into the P*sto-6*::*wCherry* construct to construct a bi-cistronic expression vector. A series of bi-cistronic expression vectors were generated by

substitution of the promoter fragments described above. *TWK-18(gf)* cDNA was PCR amplified with OZM2376 (AAG GAT CCA AAT GGC GAT TGT TGC) and OZM2377 (TTG GAT CCA CTA GAT GTC ATG CTC TAG) using pCFJ70 as a template and inserted to bi-cistronic vectors. *wCherry* (a modified version of *mCherry* codon-optimized for expression in *C. elegans*) provided by A. Desai (University of California, San Diego), was used as the bi-cistronic expression reporter. *unc-7* cDNA was amplified by PCR using OZM412 (GCG GGA TCC GTC AGT CTA TCG TCC CTT GAC CGT) and OZM413 (GCC GGA TCC CCA TGC TCG GCT CCT CCA GCA ATC C) with cDNA library (Vidal cDNA library) as template. *unc-9* cDNA was amplified by PCR using OZM417 (GGG GAT CCG GAT GAG TAT GCT ATT GTA TTA TTT CGC G) and OZM418 (GGG GAT CCT CAC ACG TCG TGC ATT TTT CCT TC) with the cDNA library as template. The sequences of resulting DNA clones were confirmed by sequencing. These cDNAs were inserted into bi-cistronic expression vectors described above to generate rescuing constructs for innexin mutants. The YFP region of YC2.12 (EallQ) was substituted with cpVenus to construct pJH1737, a calcium insensitive control for YC3.60. The same E all Q substitutions were introduced into the mtCalmodulin fragment of D3cpv by PCR mutagenesis to generate calcium-insensitive D3cpv control plasmid pJH2157.

Curvature analysis

High contrast images of crawling young adults on OP50 seeded plates were captured using a stereo-microscope or a custom built worm tracker which acquired images at 5 fps (Stephens et al., 2008). Image processing code was written in MATLAB

(Mathworks, Natick, MA). To calculate curvature of the animal, the “spine” was extracted by a modified center-line detection algorithm (Guberman et al., 2008). First the curvature of the animal’s boundary is calculated. The "tail" and the "head" are found by selecting the boundary points with the smallest (tail) and the second smallest (head) radius of curvature. The boundary is then divided into the dorsal and ventral sides. For each point inside the boundary, we find the shortest distances between the point and two sides, and if the difference between the distances is smaller than a certain threshold, the point is considered part of the spine. When all the points on the spine are extracted, the spine is re-sampled to 37 equally spaced points from head to tail. The curvatures of the points are then calculated as $k = (x'y'' - y'x'') / (x'2 + y'2)3/2$ where the discrete derivatives are defined as $f'(j) = f(j+1)-f(j-1)$ and $f''(j) = f(j+2) - 2f(j) + f(j-2)$. Images of any animal that crossed over itself were not processed.

Forward and backward movement analysis

L4 stage animals were transferred to a NGM plate seeded with a thin layer of OP50. After one minute, a two-minute movie of the crawling animal was recorded using a standard digital camera installed on a Leica MS5 dissecting microscope. Images were sampled from the movies at 1fps and processed by in-house developed ImageJ plugins. The longest distance of the outline of a detected object was calculated, and points giving this value were assigned as the head or tail positions. The anterior to posterior direction of the assigned points was manually determined and tracked automatically by the plugins afterwards to determine the direction of movements. The distance between the center points of the head-to-tail positions between two consecutive frames was calculated to

determine the status of movements. Less than 1 pixel shift in position was defined as "pausing" in this analysis. The percentage of total frames exhibiting forward motion, backward motion and pausing was calculated from the pooled image frames obtained from multiple animals of each genotype. The duration of forward and backward motion, the mean number of video frames with an animal moving in the same direction, was determined for each animal during the two-minute recording. N>10 animals for each genotype were analyzed for the averaged duration.

Electrophysiology

Membrane potentials of AVA premotor interneurons were recorded in whole-cell configuration by a Digidata 1440A and a MultiClamp 700A amplifier using the Clampex 10 software, processed with Clampfit 10 (Axon Instruments, Molecular Devices, USA). Data were digitized at 10−20 kHz and filtered at 2.6 kHz. The dissection of *C. elegans* was performed with a modified protocol described previously (Gao and Zhen, 2011). Briefly, one or two day old hermaphrodite adults were glued to a sylgard-coated coverglass covered with bath solution. The cuticle in the head region was cut along the dorsal side of the animal and pinned down to the coverglass to expose neurons of the central nervous system. All recorded animals carried two transgenes expressing two fluorescence markers: a wCherry marker driven by the P*rig-3* promoter (*hpEx2414*) and a cameleon reporter driven by P*nmr-1* promoter (*hpIs190*). The AVA neurons were identified as neurons expressing both markers.

Neuronal cell bodies were patched using fire-polished 8-12 MΩ resistant borosilicate pipettes (World Precision Instruments, USA). The pipette solution contains

(in mM): K-gluconate 115; KCl 25; $CaCl_2$ 0.1; $MgCl_2$ 5; BAPTA 1; HEPES 10; Na_2ATP 5; Na_2GTP 0.5; cAMP 0.5; cGMP 0.5, pH7.2 with KOH, ~320 mOsm. The bath solution consists of (in mM): NaCl 150; KCl 5; $CaCl_2$ 5; $MgCl_2$ 1; glucose 10; sucrose 5; HEPES 15, pH7.3 with NaOH, ~330 mOsm. Resting membrane potentials were recorded at 0 pA. Input resistance was determined measuring the voltage responses upon current injections. All experiments were performed at room temperatures (20-22^{o}C). Subsequent analysis and graphing were performed using Excel (Microsoft), Igor Pro (Wavemetrics) and Clampfit (Molecular Devices). In this study, N number represents the number of animals recorded unless specified otherwise. All data are presented as means ± SEM.

Immunofluorescent staining

Transgenic animals *unc-9(fc16)unc-7(e5); lin-39(n709);hpEx2227[*P*nmr-1::UNC-7::GFP+*P*unc-4::UNC-9- UrSL-wCherry+*P*odr-1::GFP]* were fixed in 2% paraformaldehyde for 2 hrs and processed as previously described (Finney and Ruvkun, 1990). *lin-39* eliminates VC neurons, where P*unc-4* also drives expression, to ensure that UNC-9 signals observed strictly came from the A-class motoneurons. A mouse monoclonal antibody against GFP (Roche), and a rabbit polyclonal antibody against UNC-9 (purified from the crude rabbit antisera raised against the last 77 amino acids, Chen et al., 2007) were used at 1:200 and 1:100 dilutions, respectively. Non-transgenic *lin-39(n709); unc-9(fc16) unc-7(e5)* progeny from the transgene population, serving as negative controls, showed no background staining.

Silencing, inactivation and ablation of premotor interneurons

Silencing of premotor interneurons was achieved by expressing P*nmr-1::TWK-18(gf)* to inactivate AVA, AVE, AVD and PVC, or/and P*sra-11::TWK-18(gf)* to inactivate AVB. Both constructs co-express wCherry from a bi-cistronic transcript to allow the confirmation of the transgene expression.

Ablation of premotor interneurons was achieved through a combined genetic and laser ablation approach. The pair of AVB neurons was removed at the second larval (L2) stage with a MicroPoint laser ablation system (Photonic Instruments) as previously described (Bargmann and Avery 1995). The AVB laser ablations were performed in the background of *akIs11; hpIs179; hpIs190*, a strain that expresses an integrated P*nmr-1::ICE* (human caspase, *akIs11*) to induce apoptosis in AVA, AVD, AVE and PVC (Zheng et al., 1999), P*sra-11::D3cpv* to label AVBs, and P*nmr-1::D3cpv* to monitor the absence of the rest of premotor interneurons. The removal of all premotor interneurons was confirmed by the absence of *hpIs179* and *hpIs190* fluorescence signals in all premotor interneurons 24 hours post laser ablation. Curvature analysis was performed on ablated animals at the last larval (L4) stage. A total number of 6 such animals were obtained and examined for this experiment.

Blocking the chemical synaptic output of AVA, AVD, AVE and PVC was achieved by expressing *Pnmr-1::Tetanus toxin* in *unc-7(e5)* animals. This construct co-expresses wCherry from a bi-cistronic transcript to allow the confirmation of the transgene expression.

Statistical Analysis

For calcium imaging and motion analyses, p values were calculated by the two-tailed Mann-Whitney U test. For electrophysiology analyses, two-tailed Student's t-test was applied to determine statistical differences. Statistical differences at $p < 0.05$ are considered to be significant (* $P<0.05$, ** $P<0.01$, *** $p<0.001$).

References

Bargmann, C. I. & Avery, L. Laser killing of cells in Caenorhabditis elegans. *Methods Cell Biol* **48**, 225-250 (1995).

Brockie, P.J., Mellem, J.E., Hills, T., Madsen, D.M., and Maricq, A.V. (2001). The *C. elegans* glutamate receptor subunit NMR-1 is required for slow NMDA-activated currents that regulate reversal frequency during locomotion. Neuron *31*, 617-630.

Chen, B., Liu, Q., Ge, Q., Xie, J. & Wang, Z. W. UNC-1 regulates gap junctions important to locomotion in *C. elegans*. *Curr Biol* **17**, 1334-1339 (2007).

Fei, Y.J., Romero, M.F., Krause, M., Liu, J.C., Huang, W., Ganapathy, V., and Leibach, F.H. (2000). A novel H(+)-coupled oligopeptide transporter (OPT3) from *Caenorhabditis elegans* with a predominant function as a H(+) channel and an exclusive expression in neurons. J Biol Chem *275*, 9563-9571.

Finney, M., and Ruvkun, G. (1990). The unc-86 gene product couples cell lineage and cell identity in *C. elegans*. Cell *63*, 895-905.

Gao, S., and Zhen, M. (2011). Action potentials drive body wall muscle contractions in Caenorhabditis elegans. Proc Natl Acad Sci U S A *108*, 6.

Guberman, J. M., Fay, A., Dworkin, J., Wingreen, N. S. & Gitai, Z. PSICIC: noise and asymmetry in bacterial division revealed by computational image analysis at sub-pixel resolution. *PLoS Comput Biol* **4**, e1000233 (2008).

Hille B. (2001) Ion Channels of Excitable Membranes (Sinauer, Sunderland, MA), 3rd Ed

Jospin, M., Qi, Y.B., Stawicki, T.M., Boulin, T., Schuske, K.R., Horvitz, H.R., Bessereau, J.L., Jorgensen, E.M., and Jin, Y. (2009). A neuronal acetylcholine receptor regulates the balance of muscle excitation and inhibition in Caenorhabditis elegans. PLoS Biol *7*, e1000265.

Maricq, A.V., Peckol, E., Driscoll, M., and Bargmann, C.I. (1995). Mechanosensory signalling in *C. elegans* mediated by the GLR-1 glutamate receptor. Nature *378*, 78-81.

Miller, D.M., Shen, M.M., Shamu, C.E., Burglin, T.R., Ruvkun, G., Dubois, M.L., Ghee, M., and Wilson, L. (1992). *C. elegans* unc-4 gene encodes a homeodomain protein that determines the pattern of synaptic input to specific motor neurons. Nature *355*, 841-845.

Stephens, G. J., Johnson-Kerner, B., Bialek, W. & Ryu, W. S. Dimensionality and dynamics in the behavior of *C. elegans*. *PLoS Comput Biol* **4**, e1000028 (2008).

Troemel, E.R., Chou, J.H., Dwyer, N.D., Colbert, H.A., and Bargmann, C.I. (1995). Divergent seven transmembrane receptors are candidate chemosensory receptors in *C. elegans*. Cell *83*, 207-218.

Tursun, B., Cochella, L., Carrera, I. & Hobert, O. A toolkit and robust pipeline for the generation of fosmid-based reporter genes in *C. elegans*. PLoS One 4, e4625 (2009).

Winnier, A.R., Meir, J.Y., Ross, J.M., Tavernarakis, N., Driscoll, M., Ishihara, T., Katsura, I., and Miller, D.M., 3rd (1999). UNC-4/UNC-37-dependent repression of motor neuron-specific genes controls synaptic choice in Caenorhabditis elegans. Genes Dev *13*, 2774-2786.

Zheng, Y., Brockie, P. J., Mellem, J. E., Madsen, D. M. & Maricq, A. V. Neuronal control of locomotion in *C. elegans* is modified by a dominant mutation in the GLR-1 ionotropic glutamate receptor. *Neuron* **24**, 347-361 (1999).